Published July 22, 2013

Coordinated waves of actomyosin flow and apical cell constriction immediately after wounding

Marco Antunes,[1,2] Telmo Pereira,[1,2] João V. Cordeiro,[1] Luis Almeida,[3] and Antonio Jacinto[1,2,4]

[1]Instituto de Medicina Molecular, Faculdade de Medicina da Universidade de Lisboa, 1649-028 Lisboa, Portugal
[2]Centro de Estudos de Doenças Crónicas (CEDOC), Faculdade de Ciências Médicas, Universidade Nova de Lisboa, 1169-056 Lisboa, Portugal
[3]Laboratoire Jacques-Louis Lions, Université Pierre et Marie Curie and Centre National de la Recherche Scientifique, F75252 Paris, France
[4]Instituto Gulbenkian de Ciência, 2780-156 Oeiras, Portugal

Epithelial wound healing relies on tissue movements and cell shape changes. Our work shows that, immediately after wounding, there was a dramatic cytoskeleton remodeling consisting of a pulse of actomyosin filaments that assembled in cells around the wound edge and flowed from cell to cell toward the margin of the wound. We show that this actomyosin flow was regulated by Diaphanous and ROCK and that it elicited a wave of apical cell constriction that culminated in the formation of the leading edge actomyosin cable, a structure that is essential for wound closure. Calcium signaling played an important role in this process, as its intracellular concentration increased dramatically immediately after wounding, and down-regulation of transient receptor potential channel M, a stress-activated calcium channel, also impaired the actomyosin flow. Lowering the activity of Gelsolin, a known calcium-activated actin filament–severing protein, also impaired the wound response, indicating that cleaving the existing actin filament network is an important part of the cytoskeleton remodeling process.

Introduction

Wound healing consists of a series of complex biological processes that are essential for multicellular organisms to respond to multiple environment aggressions and maintain tissue integrity. Studies both in vitro and in vivo, in vertebrate and invertebrate organisms (Gurtner et al., 2008; Garcia-Fernandez et al., 2009; Belacortu and Paricio, 2011), have identified particular responses specific to tissues and causes of injury, but also unveiled common repair mechanisms shared among different systems. Properties like the ability to sense tension changes within the tissue, repair epithelial defects, and elicit effective immune responses are coordinated and regulated in very robust ways from a very early point after injury and, most importantly, are highly conserved among different phyla. Therefore, studying wound healing in simpler model systems can shed light on fundamental processes that ultimately might prove essential to our understanding of the more complex wound healing response observed in human tissues.

Drosophila melanogaster has long been used as a model system for wound healing, in particular for simple epithelia repair (Garcia-Fernandez et al., 2009; Belacortu and Paricio, 2011). Studies in embryos and larvae have shown interesting parallels between the epithelial processes that are activated in response to damage and other well-described events occurring during different developmental stages (Wood et al., 2002; Galko and Krasnow, 2004). These similarities strongly suggest that the cellular pathways involved in the regulation of these processes are not only essential but also conserved. Specifically, wound closure processes including the actomyosin cable, cell migration, and cell shape changes and rearrangements are pivotal in assuring the cooperative action leading to reepithelialization (Garcia-Fernandez et al., 2009; Belacortu and Paricio, 2011). The actomyosin cable, a well-described structure that contributes to wound closure via a "purse-string" mechanism (Martin and Lewis, 1992; Danjo and Gipson, 1998; Wood et al., 2002; Tamada et al., 2007), assumes special importance not only due to its conserved role across species during wound healing, but also due to its function in other morphogenetic events such as in *Drosophila* dorsal closure and zebrafish epiboly (Martin and Parkhurst, 2004).

T. Pereira and J.V. Cordeiro contributed equally to this paper.

Correspondence to Antonio Jacinto: antonio.jacinto@fcm.unl.pt

Abbreviations used in this paper: Dia, Diaphanous; MLCK, myosin light chain kinase; TRPM, transient receptor potential channel M.

Supplemental Material can be found at:
http://jcb.rupress.org/content/suppl/2013/07/18/jcb.201211039.DC1.html
http://jcb.rupress.org/content/suppl/2013/08/05/jcb.201211039.DC2.html
http://jcb.rupress.org/content/suppl/2013/08/05/jcb.201211039.DC3.html

The Rockefeller University Press $30.00
J. Cell Biol. Vol. 202 No. 2 365–379
www.jcb.org/cgi/doi/10.1083/jcb.201211039

Published July 22, 2013

Nevertheless, despite the significant progress made so far, the early stages of the epithelial wound healing response are not yet fully understood in any of the model systems available. Recent studies have advanced our knowledge of these early stages, but the origins of the processes that have been identified as essential for epithelial repair such as the actomyosin cable remain elusive. One of the first tissue responses that has been described as a consequence of tissue wounding is the increase of intracellular calcium in cells that surround the wound. This response has been shown in several cell culture systems including epithelial and endothelial cell monolayers (Sammak et al., 1997; Klepeis et al., 2001; Shabir and Southgate, 2008; Chifflet et al., 2012), but also in vivo in *Xenopus* embryos (Clark et al., 2009), in *Caenorhabditis elegans* syncytial epidermal wounds (Xu and Chisholm, 2011), and in zebrafish fin fold regeneration (Yoo et al., 2012). However, the consequences of the transient elevated calcium levels in the tissue movements have remained largely unknown. Here, we use a novel wounding assay in *Drosophila* that allowed us to explore the events that precede the formation of the actomyosin cable during epithelial repair, including the dynamic analysis of calcium levels with high temporal and spatial resolution. We show that wounds in *Drosophila* pupal epithelia cause mechanical stress and trigger a dramatic increase of intracellular calcium in cells that surround the wound, which correlates with highly dynamic changes in apical actomyosin. These cytoskeletal changes lead to a wave of apical cell constriction that culminates in the assembly of the actomyosin cable. We have used tissue-specific RNAi to identify several of the players involved in this process, which includes a stress-activated calcium channel and cytoskeleton regulators.

Results

Wound healing in the pupal epithelium

To better characterize the initial phases of epithelial repair we have developed a novel wounding assay using the *Drosophila* pupal notum epithelium (Fig. S1 A), a tissue that has already been successfully used to study epithelia properties in vivo, such as epithelial polarity (Langevin et al., 2005; Bosveld et al., 2012). The notum is easily accessible and the epithelium is relatively flat, making it convenient for wounding and live imaging by using methodologies similar to the ones previously developed for *Drosophila* embryos (Wood et al., 2002). Furthermore, this tissue and stage of fly development allowed us to take advantage of tissue-specific RNAi to study the effects of knocking down genes of interest (Dietzl et al., 2007). We first set out to characterize notum epithelial repair using an E-cadherin–GFP reporter (Oda and Tsukita, 2001). After laser ablation the wound area expanded, as consequence of tissue tension release (Ma et al., 2009), but immediately initiated the cell shape changes necessary to close the wound that with our laser ablation settings had ∼40-µm diameter (Fig. S1 A). Subsequently, we used the driver *pannier-(pnr)-GAL4* (Calleja et al., 1996), which is expressed in the central notum region, to express different cytoskeletal protein markers during the resealing process. Using mCherry-Moesin as an actin reporter (Edwards et al., 1997; Millard and Martin, 2008) and Spaghetti-Squash (Sqh)-GFP as a nonmuscle myosin II marker (Royou et al., 2002), we observed an initial accumulation of these molecules in the vicinity of the wound in the first minutes after ablation (Fig. 1 and Video 1). Similarly to what has been observed in embryonic wound healing (Wood et al., 2002), the formation of an actomyosin cable is already visible at 15 min after wounding and is complete in the first 30 min. Later, cable contraction cooperates with actin-rich protrusions, such as lamellipodia and filopodia, to achieve wound closure by 3 h after wounding (Fig. 1 and Video 1). Finally, epithelial rearrangements can be observed in what constitutes a final tissue-remodeling phase (Video 1). As it was shown in other systems, pupal wounds attract immune cells (hemocytes) that are likely to be involved in clearing the wound debris (Fig. S1 B; Stramer et al., 2005). In summary, our results show that epithelial repair in the pupal notum occurs via mechanisms that are similar to wound healing in embryos and epithelial-like cell monolayers in culture.

Formation of an actomyosin cable is preceded by an actomyosin flow and a wave of cell constriction

To investigate the tissue responses before the formation of the actomyosin cable, we set out to image actomyosin dynamics and cell shape changes in the early seconds after wounding. Imaging mCherry-Moesin immediately after laser ablation using the protocol described above revealed a dramatic phenotype consisting of a pulse of new actin filaments that starts three or four cells away from the wound and flows from cell to cell toward the wound margin (Fig. 2 A and Video 2), and culminates in the formation of the actin cable at the leading edge ∼15 min after wounding (Fig. 2, A and B). We could also observe that different size wounds trigger responses of different magnitudes; there is a positive correlation between the size of the wound and the distance from the edge where the actin flows starts (Fig. S2, A and B). This response is specifically caused by the wound, as a pulse of actin filaments with such magnitude was never observed in unwounded tissue (Fig. 2 A and Fig. S3 A). Next, we tested whether this actin flow was accompanied by any corresponding changes in myosin dynamics. Analysis of the first minutes of wound healing when we expressed mCherry-Moesin and Sqh-GFP simultaneously showed a coordinated response whereby both actin and myosin flow toward the wound (Fig. 2 B and Video 3). Both flows travel in the apical region of the cells and culminate in the formation of the actomyosin purse-string before any significant reduction in wound area is observed (Fig. 2 B and Video 3). Analysis of a Z-section of cells close to the wound at different time points (Fig. 2 Bii) reveals that the actin flow moves ahead of the myosin as both move toward the wound, suggesting that the actin filaments assemble before the recruitment of the myosin.

As the ability of cells to change shape in response to different stimuli is largely dependent on actin filaments and myosin motors (He et al., 2010; Lecuit et al., 2011), we used E-cadherin–GFP to monitor the impact that the actomyosin flow had on cell shapes. Examination of the first minutes after laser

Published July 22, 2013

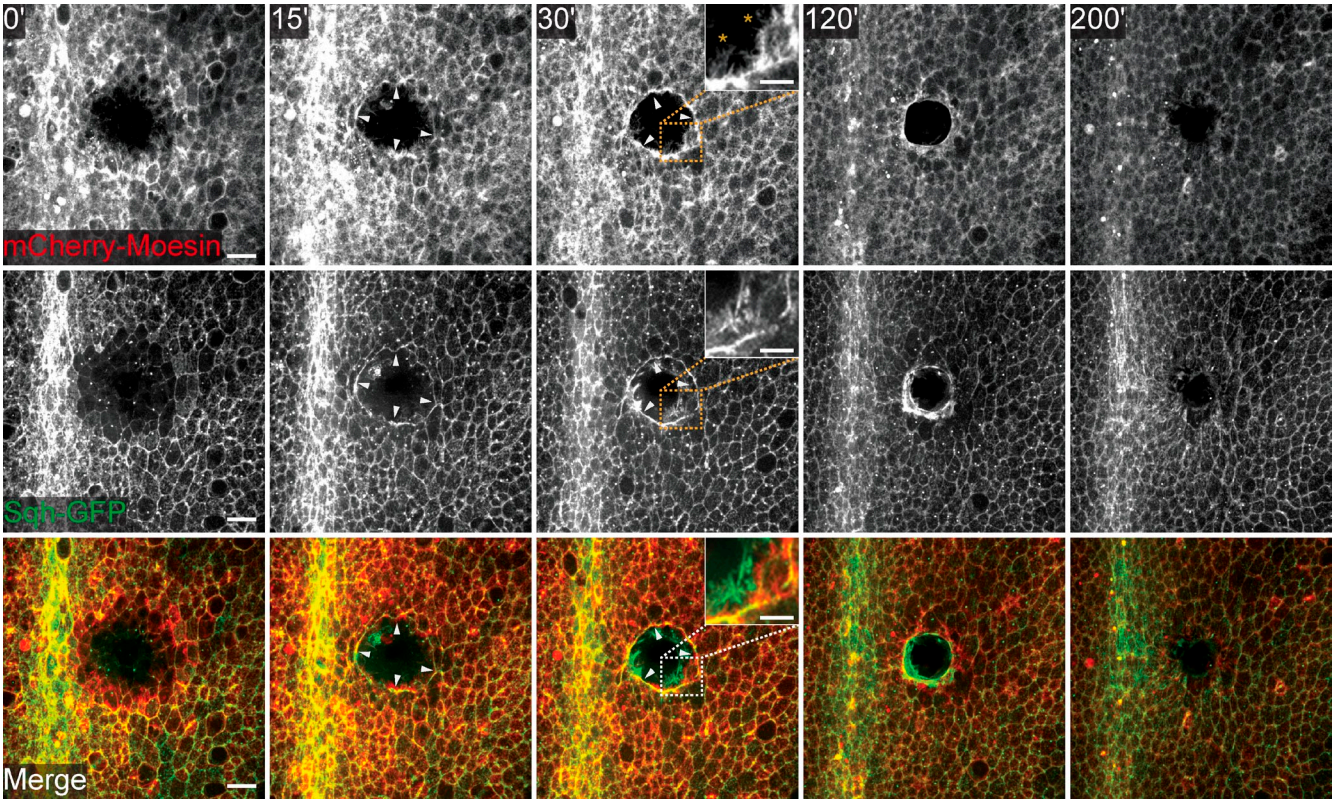

Figure 1. ***Drosophila* pupal wound healing.** Movie stills of a wounded pupal notum expressing mCherry-Moesin under the control of *pnr-GAL4* and Sqh-GFP show that pupal epithelial repair recapitulates embryonic wound healing. White arrowheads highlight the actomyosin cable. Actin-rich protrusions, such as lamellipodia and filopodia, are highlighted in the zoom panel at 30 min after wounding. Time after wounding is indicated in the top panels. Bars: (main panels) 20 µm; (insets) 10 µm.

ablation revealed a surprising tissue deformation response, which consisted in a wave of coordinated cell constriction that started a few cells away from the wound margin and moved rapidly toward the center of the wound (Fig. 2 C and Fig. S3 B), a behavior that resembles that of the actomyosin flow. The global analysis of the apical area confirmed that cells further away from the wound constrict first and subsequently distend as the next row of cells constricts. In our standard wounding assay (wound diameter = 40 µm) the first constriction occurs three or four cell rows away from the wound and the process is propagated from cell to cell until the leading edge cells contract, terminating the process (Fig. 3, A and B).

To clarify the link between the actomyosin flow and the apical constriction wave, we wounded specimens labeled with mCherry-Moesin and E-cadherin–GFP. Analysis of tissue dynamics revealed that the actin flow precedes the contraction wave; the peak of actin filament assembly in a cell occurs around 200 s before that very same cell constricts apically (Fig. 3 C and Video 4). A more detailed analysis shows that the peak of maximum actin intensity in a given row of cells, at approximately the same distance to the wound center, precedes the peak of minimum cell area of the corresponding cell row (Fig. 3, B and D). Moreover, the minimum cell area seems to correlate with the maximum myosin intensity, suggesting that the sliding of myosin motors over actin filaments is indeed the driving force behind the apical constriction wave (Fig. 3 D).

ROCK and Diaphanous down-regulation disrupt the actomyosin flow and abrogate apical cell constriction

Members of the Rho family of GTPases have been shown to regulate the cytoskeletal rearrangements that occur during epithelial repair (Wood et al., 2002). To determine whether these proteins regulate the observed actomyosin flow and wave of apical cell constriction, we knocked down Rho1, the member of the Rho GTPase family that regulates actomyosin contractility. However, expression of Rho1 dsRNA in the pupal notum using the driver *pannier-GAL4* led to lethality and no viable pupae were obtained. To circumvent this limitation we used the same method to knock down Diaphanous (Dia) and ROCK, two proteins that act downstream of Rho1 to regulate the cytoskeleton dynamics. Dia is a formin involved in de novo actin nucleation and extension of nonbranched actin filaments (Schirenbeck et al., 2005), and ROCK is a kinase that activates myosin regulatory light chain (MRLC), either directly or through the inactivation of myosin phosphatases, leading to actomyosin contractility (Narumiya et al., 1997; Ueda et al., 2002). Analysis of wounded pupae after either Dia or ROCK knockdown revealed that both the actomyosin flow and the apical constriction wave were severely affected (Fig. 4 A, Bi, and Bii; Fig. S3 C; and Video 5). The actomyosin cable was also impaired when Dia or ROCK were knocked down (Fig. 4 Biii). The strongest phenotype results from ROCK down-regulation,

Published July 22, 2013

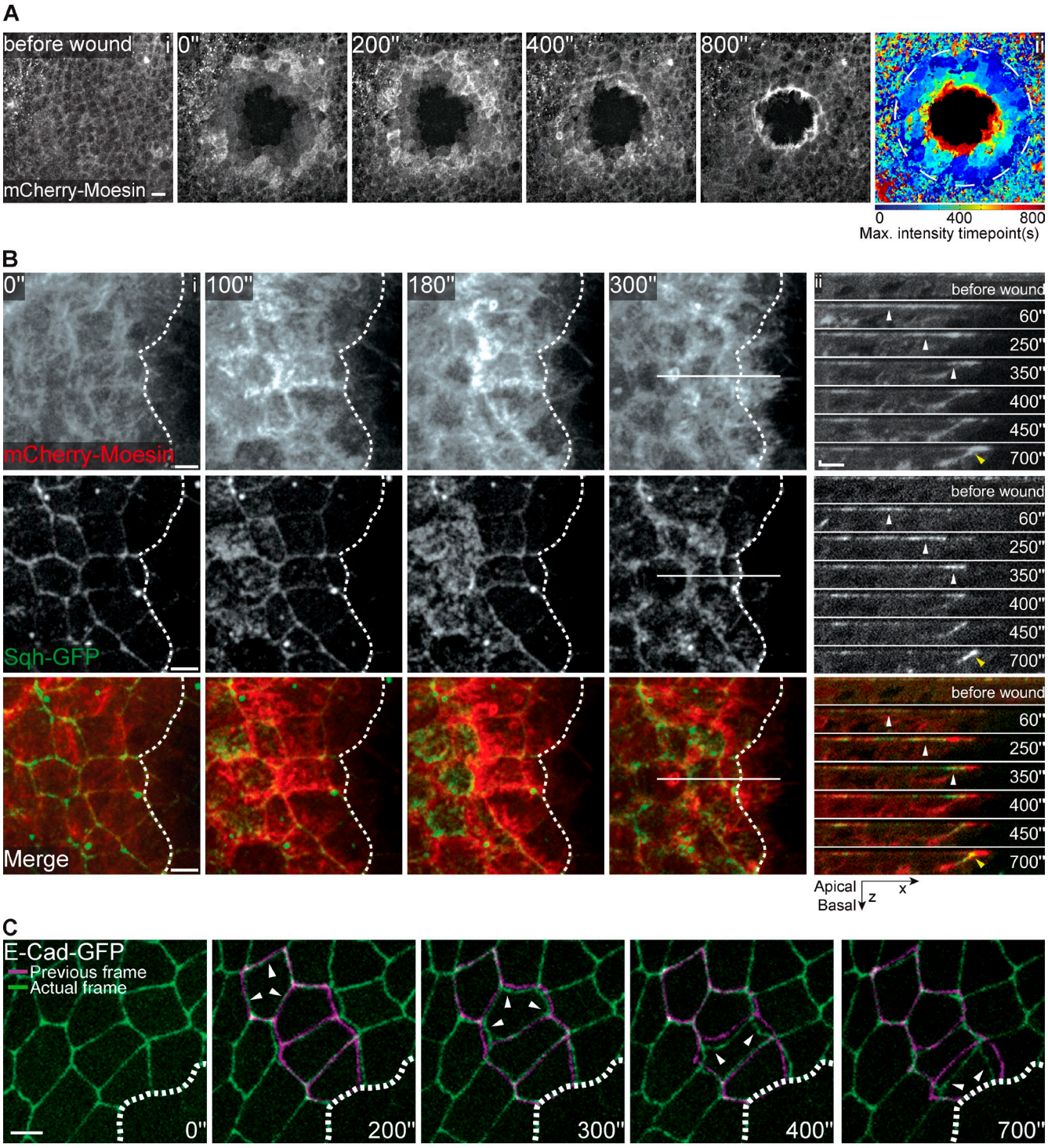

Figure 2. **The initial wound healing response consists of a pulse and flow of actomyosin and a synchronized wave of apical cell constriction.** (Ai) Movie stills of a pupal notum expressing UAS-mCherry-Moesin driven by *pnr-GAL4* show a flow of increasing actin accumulation, which is visible in the early minutes of wound healing and culminates in cable formation. Time after wounding is indicated in the panel's top left corner. (Aii) Graphic representation of the actin flow according to a color-coded time scale. The time when each pixel reaches its maximum actin intensity is color coded, ranging from early time points in dark blue to latter time points in dark red. A wild-type flow is represented by a gradient of colors, dark blue in the periphery (early maximum actin intensity) and red at the leading edge (late maximum actin intensity). Bar, 10 µm. (Bi) Movie stills of an epithelium expressing mCherry-Moesin and Sqh-GFP show that after injury actin and myosin flows progress toward the wound. Dashed lines indicate the wound margin. Horizontal line indicates the xz kymograph area shown in Fig. 2 Bii. Bar, 5 µm. (Bii) xz kymograph shows that the myosin follows the actin flow in the early minutes of wound healing. White arrowheads indicate the position of the maximum of myosin intensity at each time point. Both flows are apical and culminate in the formation of the actomyosin purse-string (yellow arrowhead). Bars: (x) 5 µm; (z) 2 µm. (C) Movie stills of the early stages of wound healing in a pupal notum expressing E-cadherin–GFP. A wave of synchronized cell constriction can be seen starting as early as 200 s after wounding and rapidly progressing toward the wound margin. Cells highlighted by white arrowheads are at the leading edge of the contraction wave. The magenta line represents the previous frame superimposed on the actual frame (green). Time after wounding is indicated at the bottom of each panel. Bar, 5 µm.

Published July 22, 2013

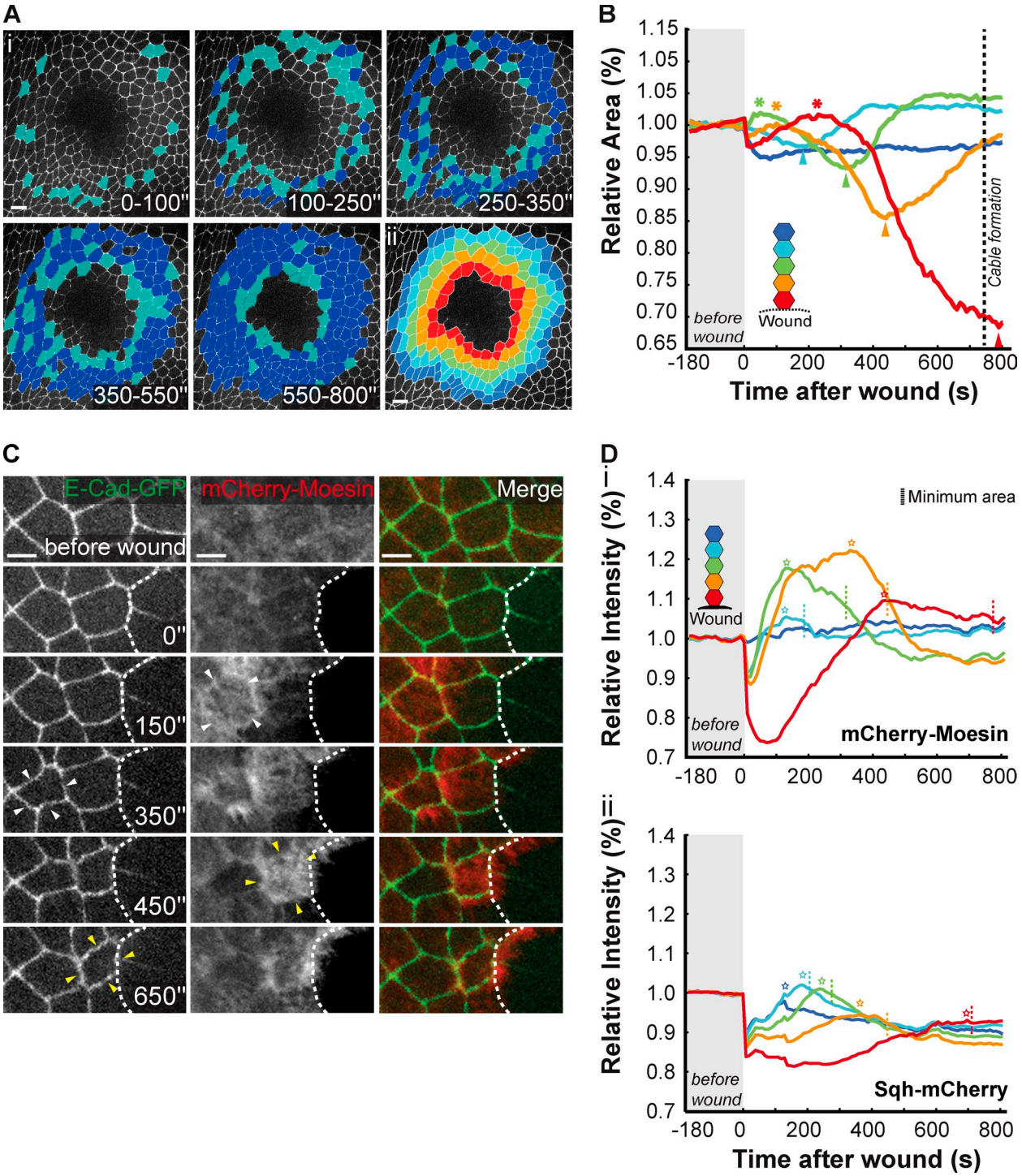

Figure 3. **Coordinated actin and myosin flows provide the driving force for apical cell constriction.** (Ai) Movie stills of the initial stages of wound healing illustrate that the early contraction wave assumes a circular shape. Cells that constrict during the indicated time intervals are highlighted in light blue. Dark blue shows all cells that have contracted since the beginning of wound healing. (Aii) Representative image of the wounded tissue shown in Ai highlighting a color code that represents distance in number of cell rows to wound. Rows close to the margin are colored in red and the following rows are colored in the sequence: yellow, green, light blue, and dark blue. Bars: (i and ii) 10 µm. (B) Graph representing changes in relative cell area during the initial stages of wound healing. Asterisks indicate the maximum area that follows the initial cell expansion. Arrowheads highlight maximum constriction of each cell row revealing that cells closer to the wound margin contract later. Color code represents distance to the wound according to Aii. (C) Stills of an E-cadherin–GFP and mCherry-Moesin movie illustrating that cell constriction follows actin assembly in progression toward the wound margin (dashed line). Bar, 5 µm. White arrowheads highlight a cell that first shows an increase in actin followed by constriction. Yellow arrowheads show a similar pattern visible in the next cell moments later. (Di) Graph representing the variation of actin intensity with time during the initial stages of wound healing. Asterisks highlight maximum actin concentration of each cell row revealing that cells closer to the wound reach their maximum actin concentration later compared with cells further away from the wound. Corresponding time points of minimum area/maximum constriction are marked with a dashed line. (Dii) Graph representing the variation of myosin intensity with time during the initial stages of wound healing. Asterisks highlight maximum myosin concentration of each cell row revealing that cells closer to the wound reach their maximum myosin concentration later. Corresponding time points of minimum area/maximum constriction are marked with a dashed line. Color code in Di and Dii correspond to Aii.

Published July 22, 2013

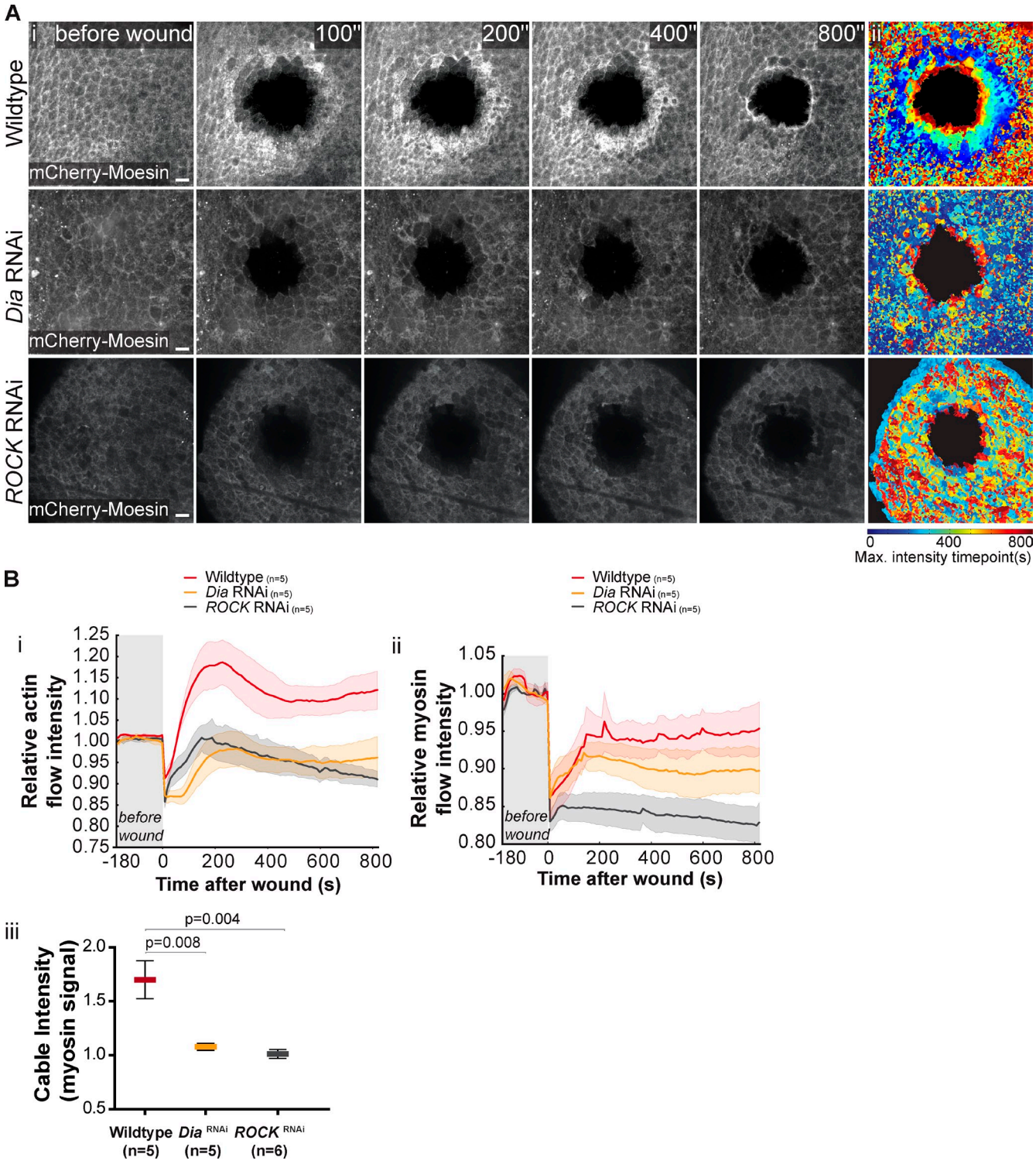

Figure 4. **Diaphanous and ROCK regulate the actomyosin flow.** (Ai) Movie stills of a pupal notum expressing UAS-mCherry-Moesin driven by *pnr-GAL4* show the flow of increasing actin concentration, which is visible in the early minutes of wound healing. Both Dia and ROCK RNAi impair the actin flow, leading to a weaker cable. (Aii) Graphic representation of the actin flow, color coded as Fig. 2 Aii. An impairment of the actin flow can be seen in the cases of Dia and ROCK RNAi. Bar, 10 µm. (Bi) Graph representing the variation of actin flow intensity in WT, Dia RNAi, and ROCK RNAi. Actin flow intensity decreases when expression of either gene is reduced. (Bii) Graph representing the variation of myosin flow intensity in WT, Dia RNAi, and ROCK RNAi. Myosin flow intensity decreases when expression of either gene is down-regulated. ROCK knockdown is particularly effective in reducing myosin concentration. Shadows represent the SEM for each curve. (Biii) Quantification of myosin cable intensity after wounding in WT, Dia RNAi–, and ROCK RNAi–expressing tissues reveals that the cable is weaker when Dia or ROCK expression is reduced (P = 0.008 and P = 0.004, respectively; Mann-Whitney test).

Published July 22, 2013

and in this case we confirmed that the wounds do not close (Fig. S4, A and B).

The actomyosin flow that we observe could result from the polymerization of filamentous actin (Dia dependent), branched actin, or a combination of both. To address this question we knocked down Arp66B, a core component of the Arp2/3 complex and known to be essential for branched actin polymerization. Arp66B down-regulation gave no phenotype (Fig. S5 A), indicating that the actomyosin flow does not result from polymerization of branched actin networks.

As ROCK is known to have several downstream targets, we confirmed the role of myosin contractility in the formation of the flow by knocking down Stretchin-MLCK (myosin light chain kinase), a more specific regulator and one of the kinases that activates myosin light chain (MLC). Stretchin-MLCK down-regulation, as Dia and ROCK, also impairs the formation of the actomyosin flow (Fig. S5 Bi), leading to the formation of a weaker cable (Fig. S5 Bii). Taken together, these results support the hypothesis that the actomyosin flow, regulated by Dia and ROCK, drives the apical constriction wave.

Anisotropy of the actomyosin flow

The anisotropy of the apical constriction wave and actomyosin flow is a surprising feature of the wound response, but closer examination of the first time-points after laser ablation revealed a possible explanation. Immediately after wounding, during the first 2–3 min, the tissue that surrounds the wound retracts as the wound expands. Cells around the wound are subjected to a sudden mechanical deformation that involves stretching in the axis parallel to the wound margin (Fig. 3 B and Fig. 5 A) and compression in the perpendicular axis. These changes in cell shape are quantifiable using the E-cadherin–GFP reporter. The adherens junctions parallel to the wound margin experience an increase in length during this expansion period that is accompanied by a gradual reduction of E-cadherin–GFP labeling relative to the length of the junction (Fig. 5, A and Bi); as junctions stretch the decrease of E-cadherin–GFP is more noticeable in junctions closer to the wound edge (Fig. 5, A and Bi, compare junction i with iii). The quantification of junctional E-cadherin levels after wounding suggests that the tissue displacement creates a gradient of tissue deformation that is established just before the actomyosin flow and correlates with its anisotropy. The extent of the tissue deformation caused by wounds depends clearly on the mechanical properties of the tissue. During the analysis of the tissue displacement in specimens where the contractility is affected due to ROCK down-regulation we could observe that the E-cadherin stretching gradient was significantly reduced (Fig. 5 Bii).

Intracellular calcium levels regulate actomyosin wave initiation and progression

Actomyosin contractility has been correlated with cytosolic calcium levels in a number of systems and tissues, and high levels of intracellular calcium have been reported as an immediate wound response (Clapham, 2007). Therefore, we wondered whether changes in intracellular calcium levels might be involved in the regulation of the actomyosin pulse and flow. To test this hypothesis we took advantage of G-CaMP3, a genetically encoded calcium probe (Nakai et al., 2001; Tian et al., 2009). Expression of G-CaMP3 under the control of *pnr*-GAL4 revealed no significant changes in calcium levels before wounding (Video 6). However, a sharp increase in intracellular calcium was detected around the wound margin immediately after wounding, but before the actomyosin flow, and rapidly spreading to areas more distal to the wound site (Fig. 6 A and Video 6). After this initial spreading the levels of cytosolic calcium decrease from the periphery to the margin of the wound, resembling the actomyosin flow. To determine whether affecting calcium transport had an effect on the actomyosin wave and subsequent actomyosin cable we tested the function of transient receptor potential channel M (TRPM), a calcium channel that has previously been shown to mediate the influx of calcium in *C. elegans* epithelia after a wound (Xu and Chisholm, 2011). Strikingly, TRPM down-regulation by RNAi led to a significant impairment of the actomyosin flow (Fig. 6, B, Ci, and Cii; and Video 5), and resulted in the formation of a weaker actomyosin cable when compared with the wild type (Fig. 6 Ciii), supporting the hypothesis that calcium signaling is necessary for these processes. The analysis of calcium levels when TRPM is down-regulated reveals that the calcium response is significantly affected (Fig. 6 D). The levels of intracellular calcium in this genetic background increased initially, but with less intensity than the wild type and decreases faster to basal levels (Fig. 6 D). This result suggests that TRPM is involved in the calcium influx but might not be the only regulator of intracellular levels of calcium in response to wounds. Down-regulation of ROCK and Dia do not show a clear reduction in calcium levels in response to wounds as TRPM, but show some specific effects. Dia closely resembles the wild-type calcium waves, whereas ROCK initially exhibits a relatively low level of intracellular calcium but its intensity decays very slowly and by the end of the experiments shows the highest levels of intracellular calcium. These results suggest that calcium influx acts upstream of both Dia and ROCK but it is likely, particularly in the case of ROCK, that there is a feedback effect on calcium. This could be due to the changes in the mechanical properties of the tissue caused by ROCK down-regulation.

When we analyzed both the calcium pulse and the actomyosin flow in the same specimens we could observe a clear spatial and temporal correlation (Fig. 7 A). By plotting the data in kymograph format (Fig. 7 B) we could observe that the actomyosin flow toward the wound edge seems to travel ahead of the calcium peak. The highest levels of actomyosin filaments are observed not in cells that have the maximum levels of intracellular calcium, but in cells that exhibit an intermediate level (Fig.7 C). At a given time point the cells that exhibit the maximum levels of intracellular calcium also show a relative decrease in the actomyosin levels (Fig.7 C) and the cells where the actomyosin flow has the highest intensity are in a region between the cells that exhibit the calcium peak and the wound edge (Fig. 7 C). As both waves move toward the wound the actomyosin flow is always ahead, closer to the wound edge (Fig. 7 A). These results suggest that calcium has an effect

Published July 22, 2013

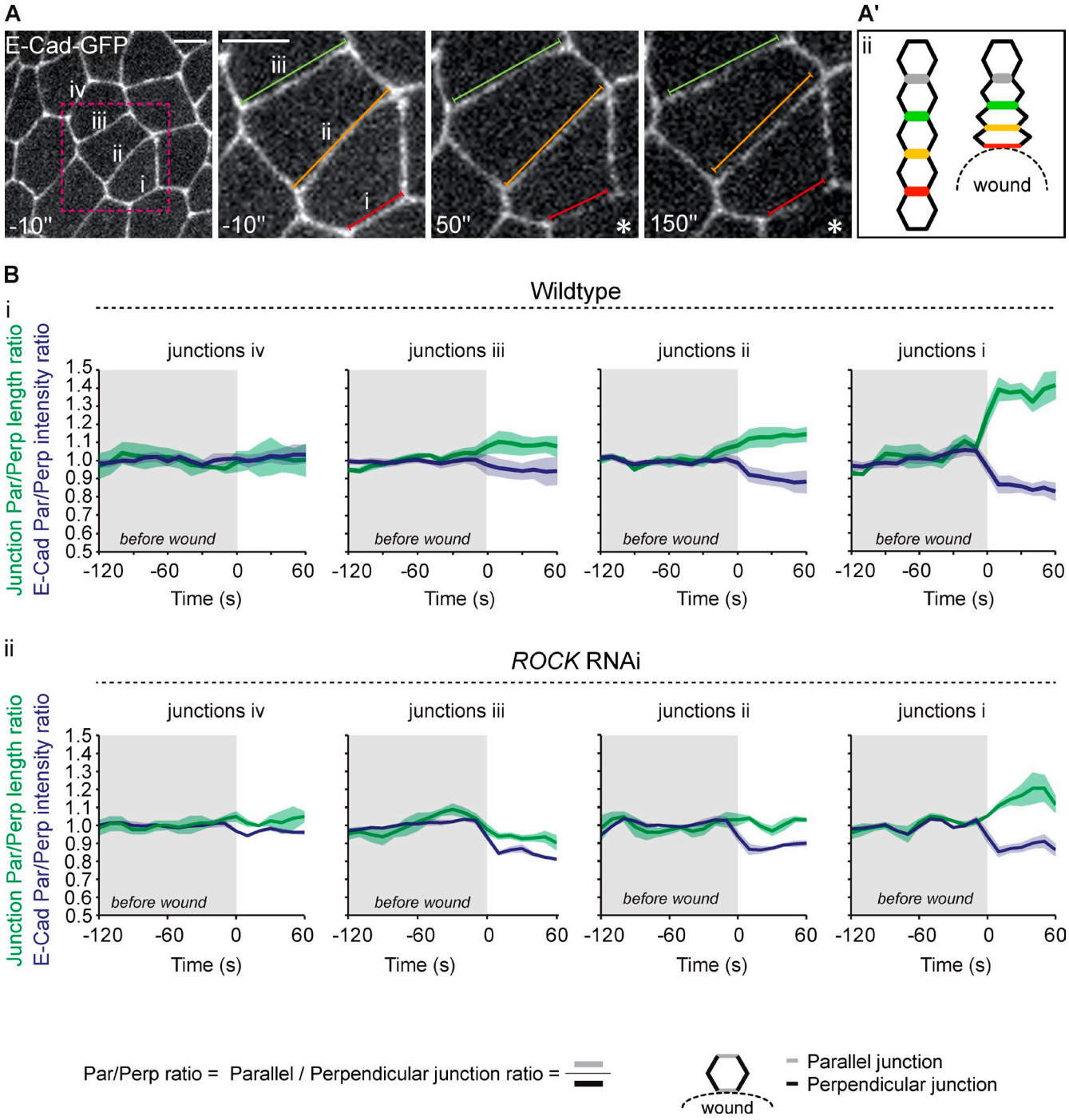

Figure 5. **Junctional E-cadherin gradients in wounds.** (A) Analysis of the first 150 s after wounding reveals that the adherens junctions closer to the wound (i–iv) initially stretch in the axis parallel to the wound and this is accompanied by a decrease in E-cadherin–GFP levels. To facilitate comparison, lines with the same color have the same length and follow the color code as in Fig. 3 Aii. Asterisks indicate the wound site. Bars, 5 µm. (A′) Diagram illustrating the changes in junctional length upon wounding. Junctions perpendicular to the wound are compressed and shortened due to tissue displacement that results from wound opening, and junctions parallel to the wound increase their length. The color code in matched with the previous panel and with Fig. 3 Aii. (Bi) Quantitative analysis of junctional length and relative E-cadherin levels in consecutive rows of cells around the wound in wild-type tissue. The green dataset represents the length ratio of parallel over perpendicular junctions, whereas the purple dataset represents the E-cadherin intensity ratio of parallel over perpendicular junctions. The proximity of junctions (i–iv) to the wound edge are as in A; junctions i are the closest and iv the most distant. Upon wounding, relative cell junction length ratio increases (junction length ratio = average parallel junctions length/average perpendicular junctions length) and relative E-cadherin levels decrease, establishing a gradient that is more pronounced at the wound margin (junctions i) and more attenuated four cell rows away from the wound margin (junctions iv). Relative junction length and E-cadherin–GFP intensity are calculated relatively to the average values before wounding. Shaded areas represent the SEM for each curve. (Bii) Analysis of junctional length and relative E-cadherin levels in ROCK RNAi tissue shows that upon ROCK down-regulation tissue displacement and E-cadherin distribution are different from wild-type.

Published July 22, 2013

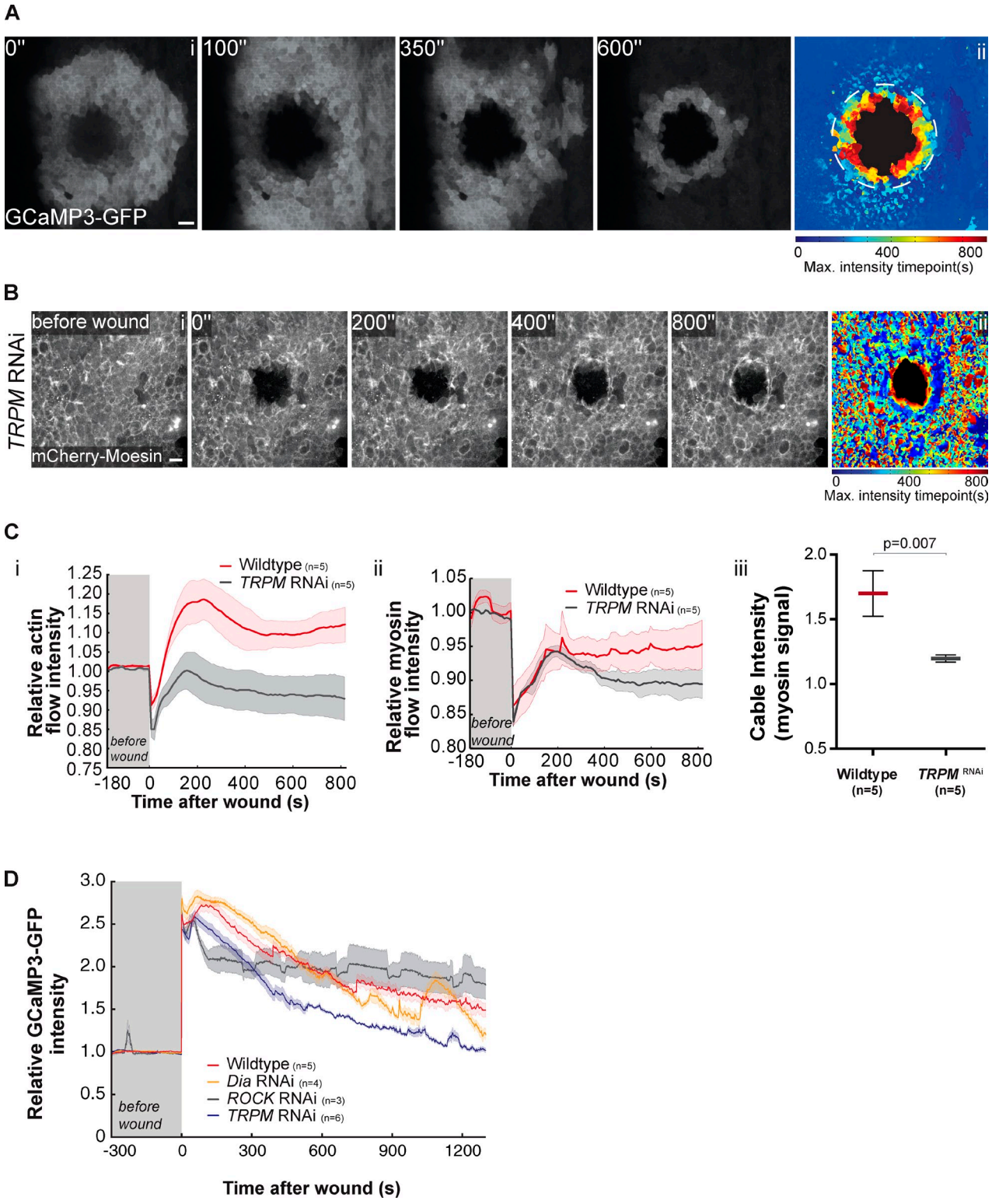

Figure 6. **Wounds cause an increase of intracellular calcium.** (Ai) Movie stills of a pupal notum expressing the calcium probe G-CaMP3-GFP driven by *pnr-GAL4* in the early seconds of wound healing. After an initial rise in intracellular calcium in the vicinity of the wound, which spreads throughout the injured tissue, a wave of high calcium levels can be observed progressing toward the wound center. (Aii) Graphic representation of the calcium wave color coded as Fig. 2 Aii. Bar, 10 µm. (B) Movie stills showing that TRPM down-regulation impairs the actin flow. (Bii) Graphic representation of the actin flow, color coded as Fig. 2 Aii. An impairment of the actin flow can be seen when TRPM is down-regulated. Bar, 10 µm. (Ci and Cii) Graphs representing the variation of actin and myosin flow intensity in WT and TRPM RNAi showing that TRPM down-regulation affects both actin and myosin flows. Shadows represent the SEM for each curve. (Ciii) Quantification of myosin cable intensity in WT and TRPM RNAi shows that this structure is weaker when TRPM expression is reduced (P = 0.007, Mann-Whitney test). (D) Graph representing GCaMP3-GFP (calcium probe) intensity in wild-type, Dia RNAi, ROCK RNAi, and TRPM RNAi. Calcium levels in Dia knockdown are similar to wild-type, whereas ROCK RNAi initially shows low levels of intracellular calcium that decay very slowly. In TRPM down-regulation the initial increase of calcium levels is impaired and it decreases faster to basal levels.

Published July 22, 2013

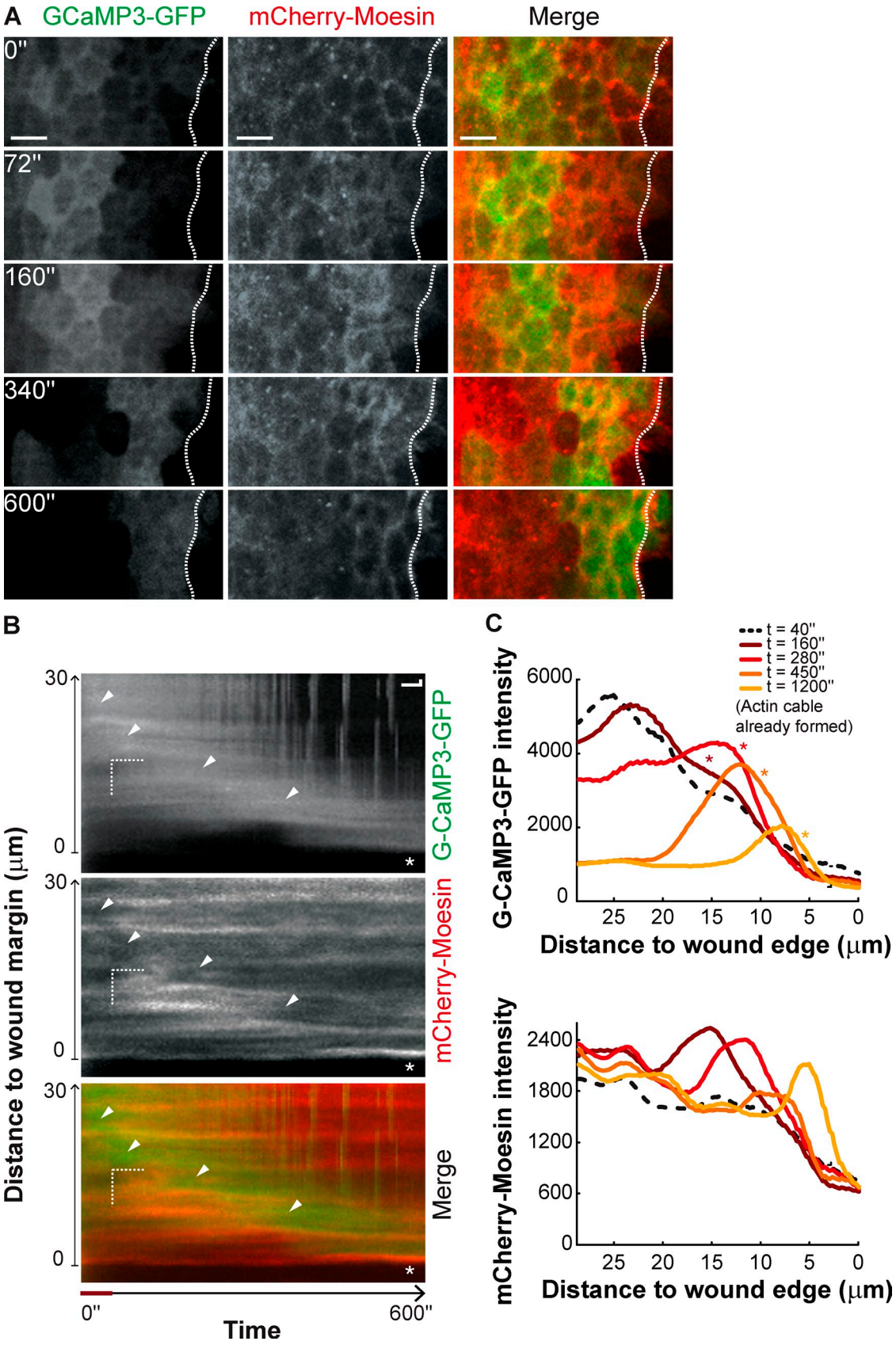

Figure 7. **Calcium wave and actin flow progress in synchrony toward the wound margin.** (A) High magnification stills of a pupal notum expressing G-CaMP3-GFP and mCherry-Moesin under the control of *pnr-GAL4* in the early seconds of wound healing. After the initial spreading, a wave of high intracellular calcium progresses toward the wound in synchrony with the actin wave, culminating in actin cable formation. A dashed white line marks the wound margin. Bar, 10 μm. (B) Kymograph showing the progression of the calcium wave (white arrowheads) immediately behind the actin flow in the early seconds

Published July 22, 2013

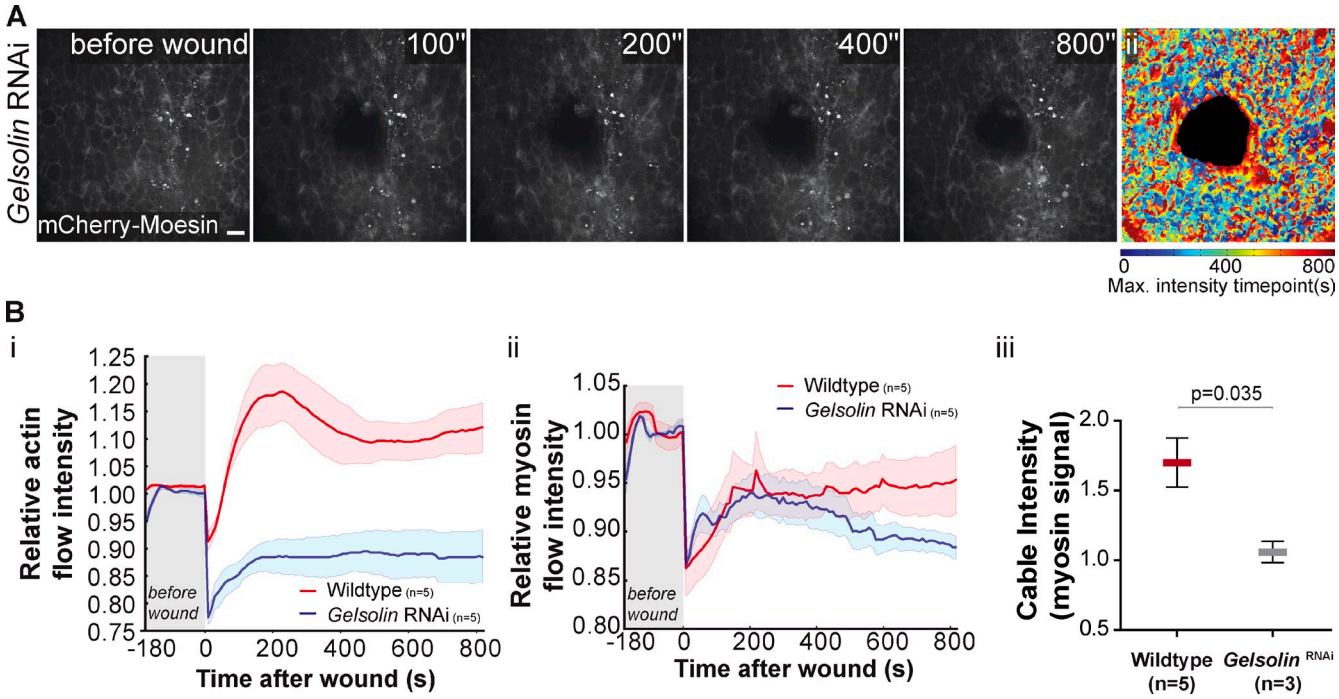

Figure 8. **Gelsolin links calcium to the cytoskeleton remodeling.** (A) Movie stills of a wounded pupal notum expressing dsRNA against Gelsolin and mCherry-Moesin driven by *pnr-GAL4*. The actin filament polymerization is not detected as in the control response (Fig. 4 A), indicating that the actin flow is disrupted by Gelsolin down-regulation. (Aii) An impairment of the actin flow can be seen on the graphic representation, color coded as Fig. 2 Aii. Bar, 10 µm. (Bi and Bii) Graphs representing the variation of actin and myosin flow intensity in WT and Gelsolin RNAi showing that upon Gelsolin down-regulation both flows are affected. Shadows represent the SEM for each curve. (Biii) Quantification of myosin cable intensity in WT and Gelsolin RNAi shows that this structure is weaker when Gelsolin expression is reduced (P = 0.035, Mann-Whitney test).

in cytoskeleton remodeling; high calcium seems to prevent actomyosin assembly, whereas intermediate levels elicit the maximum levels.

Gelsolin links calcium to cytoskeleton remodeling

Calcium is known to be important in several contexts where it can act as a second messenger in signaling cascades that require fast activation and also as a cofactor for a number of calcium-dependent proteins. To establish a direct link between calcium and the cytoskeleton we decided to test the function of Gelsolin, a calcium-dependent actin filament–severing protein known to be essential for actin cytoskeleton remodeling. Upon Gelsolin down-regulation we could observe that the actomyosin flow was severely impaired and the intensity of the cable at the wound margin was reduced (Fig. 8, A and B; and Video 5). The impact of down-regulating Gelsolin was even more dramatic than in the case of Dia or ROCK down-regulation (compare Fig. 4, A and B with Fig. 8, A and B). This phenotype indicates that immediately upon wounding and after cytosolic calcium increase, Gelsolin is essential for the initial remodeling of actin filaments that give rise to the actomyosin flow.

Discussion

The mechanisms that control the assembly of contractile actomyosin cables both in epithelial repair and tissue morphogenesis are largely unknown. Our work shows that before the cable is formed there is a pulse of actomyosin that flows to the wound edge, generating a wave of cell constriction that contributes to restoring the tissue tension and to the formation of the actomyosin cable.

The earliest event that we can observe after wound induction is the displacement of tissue that surrounds the wound (depicted graphically in Fig. 9, A and B), causing a significant deformation of the cells and their contents. The cytoskeleton networks are stretched in the axis parallel to the wound margin and compressed in the perpendicular axis. These deformations are particularly visible at the membrane level using reporters for the localization of cadherins, as shown in Fig. 5. It is likely that wound-induced deformation of the actin filaments causes changes in their structure, generating a mechanosensing mechanism. Importantly, it has been recently reported that mechanical manipulation of cells triggers actin monomer release from filaments (Higashida et al., 2013; Leckband, 2013). Another

of wound healing. First detection of the actin flow (dashed lines in Distance and Time) occurs in a region of optimal calcium concentration immediately next to a region of highest concentration. Red line in the Time axis highlights the delay between the initiation of the calcium wave and first detection of the actin flow. Asterisk indicates the actin cable. (C) Graphs representing the variation of G-CaMP3-GFP and mCherry-Moesin intensity with wound distance in the first 1,200 s of wound healing. Peaks of high intracellular calcium levels correspond to low actin intensity. The actomyosin flow is formed in cells that exhibit intermediate calcium levels and travels ahead of the calcium wave culminating in actin cable formation. Asterisks in the G-CaMP3 curves indicate position of the actin flow in the same tissue region, at the same time.

Published July 22, 2013

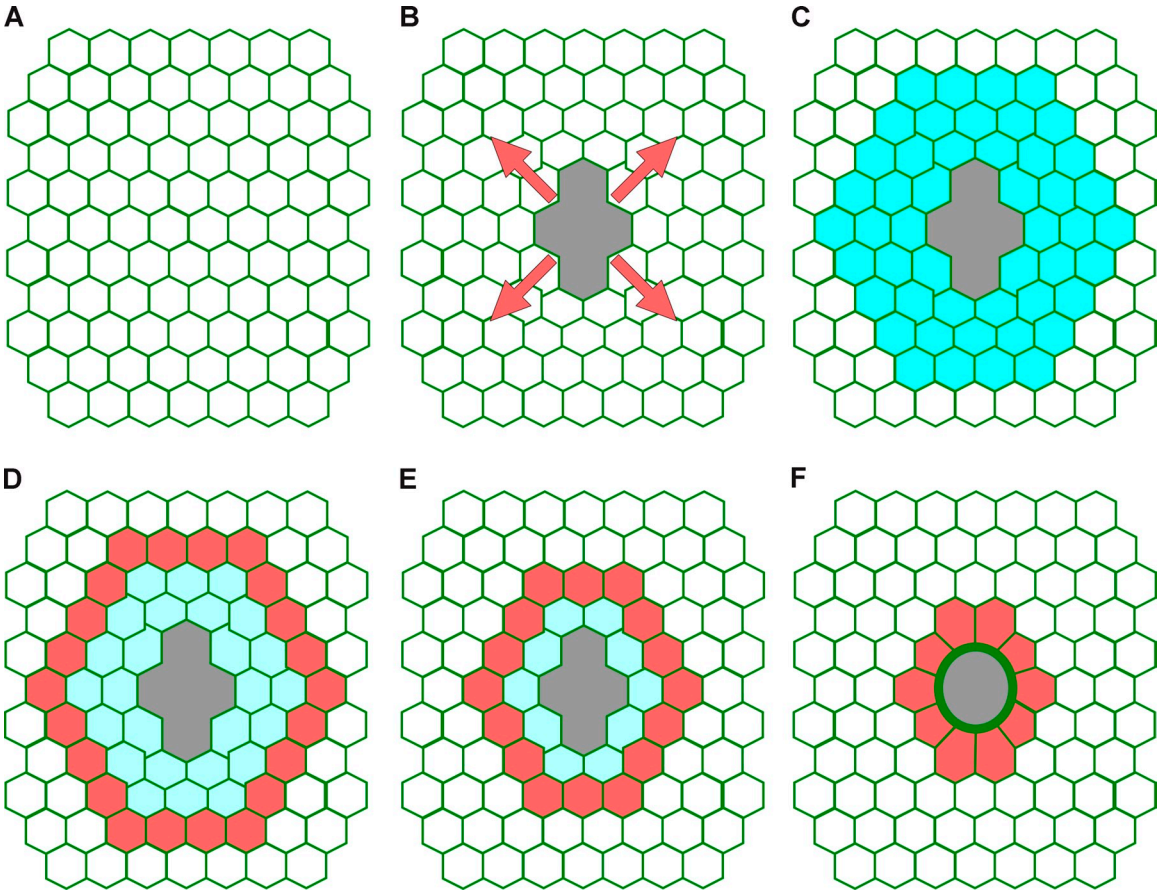

Figure 9. **Graphic model.** Schematic representation of the sequence of events that we propose to occur immediately after wounding simple epithelia. (A) Intact tissue. (B) Wounding released tension and the tissue is displaced from the wound center toward the periphery (arrows). (C) The mechanical stress leads to a burst of intracellular calcium (blue) in the cells that surround the wound. (D) The increase of intracellular calcium (blue) combined with the effects of cell and cytoskeleton deformation determine a region around the wound where a pulse of actin filaments (red) is formed. (E) The actin filaments combined with myosin motors generate an actomyosin flow (red) that travels from cell to cell from the periphery toward the wound margin. (F) When the actomyosin flow reaches the wound margin it contributes to the formation of the wound edge actomyosin cable (green).

consequence of the mechanical stress that cells suffer is a dramatic increase in intracellular calcium (Fig. 9 C), probably due to the action of stress-activated calcium channels. Down-regulation of one such channel, TRPM, results in partial impairment of the calcium influx, suggesting that *Drosophila* TRP channels could be involved in wound sensing as suggested for *C. elegans* (Xu and Chisholm, 2011). High levels of intracellular calcium affect many signaling pathways, but one of the proteins that it regulates, Gelsolin (Sun et al., 1999), seems to have an important role in the generation of new actin filaments. Gelsolin has actin filament–severing activity and its down-regulation impairs the actin flow. Our model is that the cytoskeleton deformation together with the Gelsolin-severing activity create the appropriate combination of exposed barbed ends and released actin monomers that can trigger a rapid burst of formin-dependent elongation of actin filaments (Higashida et al., 2008, 2013) that kicks off the actin flow. The distance from the wound margin at which this phenomenon occurs depends on the extent of tissue displacement (Fig. 9 D). Cells that are too far from the margin do not respond by making new filaments because they do not suffer any displacement. Cells too close to the wound do not initiate the actin flow, presumably because the cytoskeleton is so much affected that response is temporarily inhibited. This inhibition may be the result of a dramatic reduction of functional filaments caused by a combination of high tissue deformation, high levels of calcium, and Gelsolin-severing activity.

The step that follows the initial burst of actin filaments seems to be the recruitment of myosin motors that act on the filaments to initiate a flow of actomyosin and apical cell constriction that propagates toward the wound edge (Fig. 9, D–F). The actomyosin flow is likely the result of local cycles of actomyosin assembly and contraction followed by disassembly and restoration of homeostatic levels (Munro et al., 2004). This process seems to be controlled by Rho signaling and we were able to demonstrate that knocking down Dia or ROCK impairs the actomyosin flow. ROCK has the strongest phenotype, probably due to its function as a key regulator of actomyosin contractility via myosin phosphatases and MRLC. But ROCK can also have other effects through several other substrates involved in cytoskeletal regulation, including LIM kinase and ERM proteins (Amano et al., 2010). The effects of ROCK may also be exerted indirectly through its role in the regulation of adherens junctions (Simões et al., 2010). Knocking down Stretchin-MLCK results in a less dramatic phenotype but confirms that

Published July 22, 2013

regulation of myosin contractility is indeed essential for the actomyosin flow. The role played by Dia is also very central in the process. Our data suggest that this formin is the main regulator of actin polymerization in the actomyosin flow and that the Arp2/3 complex is not necessary. These results are consistent with the possibility that actin monomers released by mechanical stress may play an important role in the elongation of filaments in our experimental system. Such a mechanism has been shown to be dependent on formins and not on the Arp2/3 complex (Higashida et al., 2013). It is still unclear how Rho is activated upstream of Dia and ROCK. The simplest explanation is that Rho is also activated by calcium (Masiero et al., 1999), but it is also possible that a constitutive level of Rho activity in the tissue works together with other calcium effects on contractility, such as the activation of MLCK by calmodulin/Ca^{2+} (Citi and Kendrick-Jones, 1987).

The observation that the flow is able to travel from cell to cell indicates that the cytoskeleton of each cell is mechanically coupled to the neighbors (Martin et al., 2010). It also suggests that the force generated by the constriction wave may contribute to the successive extension of filaments not only inside each cells but also from one cell to another when the constriction wave reaches the membrane, for instance by triggering actin monomer release and activation of formins in the neighboring cell. The particular orientation of the actomyosin flow, from the periphery to the wound edge, is an unforeseen characteristic of the wound response. However, the inverse correlation between relative levels of junctional E-cadherin and proximity to the wound edge is a possible explanation to the directionality of the flow, as it has recently been shown that levels of junctional E-cadherin can direct actomyosin flows during developmental morphogenetic events (Rauzi et al., 2010; Lecuit et al., 2011; Levayer et al., 2011). An alternative but related explanation for the anisotropy of the flow is that the initial tissue displacement caused by the wound creates a gradient of cytoskeleton deformation with high deformation at the wound edge and low deformation away from the wound, at the site where flow starts. This gradient may create the appropriate conditions to activate the extension of filaments always in the direction where the cytoskeleton is more deformed, that is toward the wound edge. According to this view the apical constriction wave may also contribute to reinforce the directionality as it induces more deformation in the same direction of the flow. Interestingly, we observe that the actomyosin flow correlates with low/intermediate levels of calcium, whereas in cells where the calcium reaches the highest levels there seems to be an inhibition of actomyosin filament polymerization (Fig. 7 C). This correlation suggests that calcium has an instructive function in the propagation of the actomyosin flow. However, it is also possible that calcium plays a more permissive role and other mechanisms such as mechanical stress–induced polymerization are the key driving forces. In that scenario the appropriate range of intracellular calcium concentration would be necessary but not sufficient for the propagation of the flow.

Our results show that the epithelial response to wounds involves a high level of coordination between the cell machinery responsible for sensing changes in tissue biomechanical properties, calcium signaling, and the actin cytoskeleton. This response occurs immediately after injury and is the starting point of a complex sequence of cell behaviors that lead to restoration of tissue tension and integrity.

Materials and methods

Fly lines and genetics

Flies were cultured on standard conditions. Crosses were performed at 25 or at 29°C to maximize RNAi expression using the UAS/GAL4 system (Brand and Perrimon, 1993). For actin flow analysis a recombinant between *w;; pnr-GAL4* (Calleja et al., 1996) and *w;; UAS-mCherry-Moesin* (Millard and Martin, 2008; Lecuit et al., 2011) was used: *w;; pnrGAL4, UAS-mCherry-Moesin/TM6b*. To analyze the myosin flow, *yw; sqh-Sqh-GFP* (Royou et al., 2002) and *yw; sqh-Sqh-mCherry* (Martin et al., 2009) pupae were used. To address the link between apical cell constriction and actin accumulation, *w; ubi-E-Cadherin-GFP* flies (Oda and Tsukita, 2001) were crossed with the *w;; pnr-GAL4, UAS-mCherry-Moesin/TM6b* recombinant described above and *w; ubi-E-Cadherin-GFP/+; pnr-GAL4, UAS-mCherry-Moesin/+* pupae were selected. Imaging a pupal notum expressing *UAS-Lifeact-GFP* under the control of *pnrGAL4* confirmed our *UAS-mCherry-Moesin* observations. Additionally, no similar phenotype was observed in tissues expressing either *UAS-GFP* or *UAS-mCherry* alone under the control of *pnrGAL4*, indicating that this is indeed an actin-specific process.

For actin flow analysis in Rho1 knockdown, a *UAS-Rho1^{RNAi}* VALIUM10 TRiP (generated by Transgenic RNAi Project and obtained from Bloomington *Drosophila* Stock Center [Bloomington, IN]) fly line (Ni et al., 2009) was crossed with *w;; pnr*-GAL4, UAS-mCherry-Moesin/TM6b (no viable pupae were obtained).

For Dia and ROCK knockdown, *UAS-Dia^{RNAi}* and *UAS-ROCK^{RNAi}* VALIUM10 TRiP fly lines (all VALIUM TRiP fly lines were generated by Transgenic RNAi Project and obtained from Bloomington *Drosophila* Stock Center) were crossed with *w;; pnr-GAL4, UAS-mCherry-Moesin/TM6b* for actin flow analysis, with *w; sqh-Sqh-GFP; pnr-GAL4/TM6b* for myosin flow analysis and *w; ubi-E-Cadherin-GFP; pnr-GAL4/TM6b* for apical constriction analysis. For Dia and ROCK phenotype confirmation, *UAS-Dia^{RNAi}* and *UAS-ROCK^{RNAi}* KK VDRC (Vienna *Drosophila* RNAi Center, Vienna, Austria) fly lines were used (Dietzl et al., 2007).

Actin flow analysis in Arp66B and Stretchin-MLCK knockdowns was performed using *UAS-Arp66B^{RNAi}* VALIUM20 and *UAS-Stretchin-MLCK^{RNAi}* VALIUM10 TRiP fly lines crossed with *w;; pnr-GAL4, UAS-mCherry-Moesin/TM6b*.

For TRPM down-regulation, two different *UAS-TRPM^{RNAi}* VALIUM1 (Ni et al., 2009) TRiP fly lines were used and crossed with *w;; pnr-GAL4, UAS-mCherry-Moesin/TM6b* for actin flow analysis, with *w; sqh-Sqh-GFP; pnr-GAL4/TM6b* for cable quantification and *w; ubi-E-Cadherin-GFP; pnr-GAL4/TM6b* for apical constriction analysis.

Gelsolin down-regulation was performed using a *UAS-Gel^{RNAi}* VALIUM1 (Ni et al., 2009) TRiP fly line.

To evaluate intracellular calcium levels during wound healing we used the genetically encoded calcium indicator, *UAS-G-CaMP3* (Tian et al., 2009), crossed with *pnr-GAL4*. To assess the correlation between calcium levels and the actin flow, *w; UAS-G-CaMP3/+; pnr-GAL4, UAS-mCherry-Moesin/+* pupae were used.

To track hemocyte recruitment to the wound, we labeled simultaneously macrophages and the epithelium using *w; srpHemoGAL4, UAS-Src-eGFP, ubi-E-Cadherin-GFP* pupae.

All experiments were performed either at 25 or 29°C to maximize RNAi expression using the UAS/GAL4 system (Brand and Perrimon, 1993).

Wounding assay

Pupae were staged at 13 h APF (after puparium formation; Madhavan and Madhavan, 1980; Bainbridge and Bownes, 1981) and mounted on double-sided tape stuck to a slide. The anterior part of the puparium, covering the head and the notum, was removed, exposing the notum epithelia. A small drop of Halocarbon 700 oil (Sigma-Aldrich) was added in order to improve image quality. Two spacers made of five coverslips each were used as bridge for a coverslip placed on top of the notum. Wounds were made using a MicroPoint (Andor Technology) UV nitrogen-pumped dye laser (435 nm) coupled to a Nikon/Andor Revolution spinning disk system allowing immediate imaging after ablation.

Published July 22, 2013

Imaging and data processing

Images were acquired at 25°C on a spinning disk imaging system (Revolution XD; Andor Technology) equipped with an EMCCD camera (iXon 897; Andor Technology) coupled to a microscope (Eclipse Ti-E; Nikon) with a Plan Apo VC PFS 60× objective (NA 1.40; Nikon). This system, controlled by iQ software (Andor Technology), is suited for fast in vivo time-lapse microscopy allowing Z-stack acquisition every 10 s (2 s for calcium). After data acquisition, raw images were preprocessed in ImageJ (National Institutes of Health) to generate maximum intensity projections and bleaching correction. Hemocyte cells were tracked every 30 s using the "Manual Tracking" ImageJ plugin. For image segmentation E-cadherin–GFP, images were analyzed using a semi-automatic segmentation script made in MATLAB. Each image was smoothed with a Gaussian low-pass filter (size and sigma of 5), and its background was removed (Gaussian low-pass filtered image with filter size and sigma of 30). The operations, morphological reconstruction, and morphological opening were performed to remove small clusters of pixels and to remove gaps in the edges. Cell boundaries were obtained with watershed lines using Meyer's watershed algorithm (Meyer, 1994). This algorithm scans the grayscale image pixels to find a minima set and each minimum gets a unique label. Each label corresponds to a cell and it gets expanded (flooded) until it reaches another label or a boundary cell membrane. Pixels that remain unlabeled correspond to cell contours. Cell boundaries not detected automatically were added manually. A MATLAB function was used to obtain surface area, mean fluorescence intensity (mCherry-Moesin and Sqh-GFP), and position of the center of mass for each cell over time. In each experiment, segmented cells were divided in cell rows according to their distance to the wound edge. Area and fluorescence intensity plots were obtained by averaging the values of each cell row. All values were normalized to average values before wound. The sequence of images used to generate color-coded time plots of actin intensity were filtered in order to reduce noise, either in space (averaging filter with size 5) or in time (moving average of three images). The time point at which each pixel reaches its maximum fluorescence intensity was calculated and represented in a color-coded image ranging from 0 to 800 s.

Junction length and E-cadherin–GPF intensity quantification was performed manually using ImageJ. A line width of 5 pixels was used to average errors. Results were corrected for bleaching and normalized for the values before wound. Length and intensity ratios were calculated by dividing the values of the junctions parallel to the wound axis by the perpendicular junctions.

Kymographs were made in ImageJ, using a line with width of 3 pixels. Actin and myosin flows were tracked using a MATLAB script that tracks the maximum fluorescence intensity of the moving flow over time. For each time point the script scans the intensities along a radius from the center of the image to its limits, within 30 pixel intervals (average cell size). This scan is performed for the whole field by rotating the radial scan in steps of 1 degree and for 360 degrees. The intensity value displayed for each time point is the average of the maximum intensities of all radial scans. All values were normalized to average values before wounding. Average cable fluorescence intensity (Sqh-GFP or mCherry-Moesin) was obtained using measurement tools in ImageJ with a line width of 4 pixels on top of the cable. Cable quantification was done at a time point at which the cable was already assembled but no wound reduction could be detected. Values were normalized to average fluorescence intensity away from the wound.

Statistics

Statistical analysis was performed using Prism (GraphPad Software). Error bars in graphs correspond to the SEM. Pearson coefficient was calculated using the nonparametric Mann-Whitney test.

Online supplemental material

Fig. S1 A shows a dissected pupa and magnifications of a notum epithelium labeled with E-cadherin–GFP before and after wounding. Fig. S1 B shows hemocyte recruitment toward a wound in the pupal notum. Fig. S2 shows actin flow and apical constriction wave dependence on wound size. Fig. S3 shows that the actomyosin flow is a consequence of the wound and that this response is impaired upon Dia, ROCK, and TRPM down-regulation. Fig. S4 shows wound closure failure when ROCK is down-regulated. Fig. S5 shows that Stretchin-MLCK but not Arp66B regulates the actin flow and cable formation. Video 1 shows wound closure in a wild-type pupal epithelium. Video 2 shows the actin flow upon wounding. Video 3 shows the actomyosin flow culminating in cable formation at the wound edge. Video 4 shows the actomyosin flow leading to the apical cell constriction wave. Video 5 shows actin flow impairment upon Dia, ROCK, TRPM, and Gelsolin down-regulation. Video 6 shows calcium dynamics immediately after wounding. Online supplemental material is available at http://www.jcb.org/cgi/content/full/jcb.201211039/DC1.

We would like to thank William Razzell for sharing unpublished data; Rita Mateus, Lara Carvalho, and Nina Matova for helpful discussions; the TRiP at Harvard Medical School (NIH/NIGMS R01-GM084947) for providing transgenic RNAi fly stocks used in this study; and Bloomington *Drosophila* Stock Center for other fly lines.

We are grateful for funding from Fundação para a Ciência e a Tecnologia (SFRH/BD/41884/2007), Human Frontier Science Program (RGP/2007), and European Research Council (2007-StG-208631).

Submitted: 6 November 2012
Accepted: 14 June 2013

References

Amano, M., M. Nakayama, and K. Kaibuchi. 2010. Rho-kinase/ROCK: A key regulator of the cytoskeleton and cell polarity. *Cytoskeleton (Hoboken)*. 67:545–554. http://dx.doi.org/10.1002/cm.20472

Bainbridge, S.P., and M. Bownes. 1981. Staging the metamorphosis of *Drosophila melanogaster*. *J. Embryol. Exp. Morphol.* 66:57–80.

Belacortu, Y., and N. Paricio. 2011. *Drosophila* as a model of wound healing and tissue regeneration in vertebrates. *Dev. Dyn.* 240:2379–2404. http://dx.doi.org/10.1002/dvdy.22753

Bosveld, F., I. Bonnet, B. Guirao, S. Tlili, Z. Wang, A. Petitalot, R. Marchand, P.-L. Bardet, P. Marcq, F. Graner, and Y. Bellaïche. 2012. Mechanical control of morphogenesis by Fat/Dachsous/Four-jointed planar cell polarity pathway. *Science*. 336:724–727. http://dx.doi.org/10.1126/science.1221071

Brand, A.H., and N. Perrimon. 1993. Targeted gene expression as a means of altering cell fates and generating dominant phenotypes. *Development*. 118:401–415.

Calleja, M., E. Moreno, S. Pelaz, and G. Morata. 1996. Visualization of gene expression in living adult *Drosophila*. *Science*. 274:252–255. http://dx.doi.org/10.1126/science.274.5285.252

Chifflet, S., C. Justet, J.A. Hernández, V. Nin, C. Escande, and J.C. Benech. 2012. Early and late calcium waves during wound healing in corneal endothelial cells. *Wound Repair Regen.* 20:28–37. http://dx.doi.org/10.1111/j.1524-475X.2011.00749.x

Citi, S., and J. Kendrick-Jones. 1987. Regulation of non-muscle myosin structure and function. *Bioessays*. 7:155–159. http://dx.doi.org/10.1002/bies.950070404

Clapham, D.E. 2007. Calcium signaling. *Cell*. 131:1047–1058. http://dx.doi.org/10.1016/j.cell.2007.11.028

Clark, A.G., A.L. Miller, E. Vaughan, H.-Y.E. Yu, R. Penkert, and W.M. Bement. 2009. Integration of single and multicellular wound responses. *Curr. Biol.* 19:1389–1395. http://dx.doi.org/10.1016/j.cub.2009.06.044

Danjo, Y., and I.K. Gipson. 1998. Actin 'purse string' filaments are anchored by E-cadherin-mediated adherens junctions at the leading edge of the epithelial wound, providing coordinated cell movement. *J. Cell Sci.* 111:3323–3332.

Dietzl, G., D. Chen, F. Schnorrer, K.C. Su, Y. Barinova, M. Fellner, B. Gasser, K. Kinsey, S. Oppel, S. Scheiblauer, et al. 2007. A genome-wide transgenic RNAi library for conditional gene inactivation in *Drosophila*. *Nature*. 448:151–156. http://dx.doi.org/10.1038/nature05954

Edwards, K.A., M. Demsky, R.A. Montague, N. Weymouth, and D.P. Kiehart. 1997. GFP-moesin illuminates actin cytoskeleton dynamics in living tissue and demonstrates cell shape changes during morphogenesis in *Drosophila*. *Dev. Biol.* 191:103–117. http://dx.doi.org/10.1006/dbio.1997.8707

Galko, M.J., and M.A. Krasnow. 2004. Cellular and genetic analysis of wound healing in *Drosophila* larvae. *PLoS Biol.* 2:E239. http://dx.doi.org/10.1371/journal.pbio.0020239

Garcia-Fernandez, B., I. Campos, J.A. Geiger, A.C. Santos, and A. Jacinto. 2009. Epithelial resealing. *Int. J. Dev. Biol.* 53:1549–1556. http://dx.doi.org/10.1387/ijdb.072308bg

Gurtner, G.C., S. Werner, Y. Barrandon, and M.T. Longaker. 2008. Wound repair and regeneration. *Nature*. 453:314–321. http://dx.doi.org/10.1038/nature07039

He, L., X. Wang, H.L. Tang, and D.J. Montell. 2010. Tissue elongation requires oscillating contractions of a basal actomyosin network. *Nat. Cell Biol.* 12:1133–1142. http://dx.doi.org/10.1038/ncb2124

Higashida, C., S. Suetsugu, T. Tsuji, J. Monypenny, S. Narumiya, and N. Watanabe. 2008. G-actin regulates rapid induction of actin nucleation by mDia1 to restore cellular actin polymers. *J. Cell Sci.* 121:3403–3412. http://dx.doi.org/10.1242/jcs.030940

Published July 22, 2013

Higashida, C., T. Kiuchi, Y. Akiba, H. Mizuno, M. Maruoka, S. Narumiya, K. Mizuno, and N. Watanabe. 2013. F- and G-actin homeostasis regulates mechanosensitive actin nucleation by formins. *Nat. Cell Biol.* 15:395–405. http://dx.doi.org/10.1038/ncb2693

Klepeis, V.E., A. Cornell-Bell, and V. Trinkaus-Randall. 2001. Growth factors but not gap junctions play a role in injury-induced Ca2+ waves in epithelial cells. *J. Cell Sci.* 114:4185–4195.

Langevin, J., M.J. Morgan, J.B. Sibarita, S. Aresta, M. Murthy, T. Schwarz, J. Camonis, and Y. Bellaïche. 2005. *Drosophila* exocyst components Sec5, Sec6, and Sec15 regulate DE-Cadherin trafficking from recycling endosomes to the plasma membrane. *Dev. Cell*. 9:365–376. http://dx.doi.org/10.1016/j.devcel.2005.07.013

Leckband, D. 2013. Formin' cables under stress. *Nat. Cell Biol.* 15:345–346. http://dx.doi.org/10.1038/ncb2715

Lecuit, T., P.-F. Lenne, and E. Munro. 2011. Force generation, transmission, and integration during cell and tissue morphogenesis. *Annu. Rev. Cell Dev. Biol.* 27:157–184. http://dx.doi.org/10.1146/annurev-cellbio-100109-104027

Levayer, R., A. Pelissier-Monier, and T. Lecuit. 2011. Spatial regulation of Dia and Myosin-II by RhoGEF2 controls initiation of E-cadherin endocytosis during epithelial morphogenesis. *Nat. Cell Biol.* 13:529–540. http://dx.doi.org/10.1038/ncb2224

Ma, X., H.E. Lynch, P.C. Scully, and M.S. Hutson. 2009. Probing embryonic tissue mechanics with laser hole drilling. *Phys. Biol.* 6:036004. http://dx.doi.org/10.1088/1478-3975/6/3/036004

Madhavan, M.M., and K. Madhavan. 1980. Morphogenesis of the epidermis of adult abdomen of *Drosophila*. *J. Embryol. Exp. Morphol.* 60:1–31.

Martin, P., and J. Lewis. 1992. Actin cables and epidermal movement in embryonic wound healing. *Nature*. 360:179–183. http://dx.doi.org/10.1038/360179a0

Martin, P., and S.M. Parkhurst. 2004. Parallels between tissue repair and embryo morphogenesis. *Development*. 131:3021–3034. http://dx.doi.org/10.1242/dev.01253

Martin, A.C., M. Kaschube, and E.F. Wieschaus. 2009. Pulsed contractions of an actin-myosin network drive apical constriction. *Nature*. 457:495–499. http://dx.doi.org/10.1038/nature07522

Martin, A.C., M. Gelbart, R. Fernandez-Gonzalez, M. Kaschube, and E.F. Wieschaus. 2010. Integration of contractile forces during tissue invagination. *J. Cell Biol.* 188:735–749. http://dx.doi.org/10.1083/jcb.200910099

Masiero, L., K.A. Lapidos, I. Ambudkar, and E.C. Kohn. 1999. Regulation of the RhoA pathway in human endothelial cell spreading on type IV collagen: role of calcium influx. *J. Cell Sci.* 112:3205–3213.

Meyer, F. 1994. Topographic distance and watershed lines. *Signal Process.* 38:113–125. http://dx.doi.org/10.1016/0165-1684(94)90060-4

Millard, T.H., and P. Martin. 2008. Dynamic analysis of filopodial interactions during the zippering phase of *Drosophila* dorsal closure. *Development*. 135:621–626. http://dx.doi.org/10.1242/dev.014001

Munro, E., J. Nance, and J.R. Priess. 2004. Cortical flows powered by asymmetrical contraction transport PAR proteins to establish and maintain anterior-posterior polarity in the early *C. elegans* embryo. *Dev. Cell*. 7:413–424. http://dx.doi.org/10.1016/j.devcel.2004.08.001

Nakai, J., M. Ohkura, and K. Imoto. 2001. A high signal-to-noise Ca(2+) probe composed of a single green fluorescent protein. *Nat. Biotechnol.* 19:137–141. http://dx.doi.org/10.1038/84397

Narumiya, S., T. Ishizaki, and N. Watanabe. 1997. Rho effectors and reorganization of actin cytoskeleton. *FEBS Lett.* 410:68–72. http://dx.doi.org/10.1016/S0014-5793(97)00317-7

Ni, J.-Q., L.-P. Liu, R. Binari, R. Hardy, H.-S. Shim, A. Cavallaro, M. Booker, B.D. Pfeiffer, M. Markstein, H. Wang, et al. 2009. A *Drosophila* resource of transgenic RNAi lines for neurogenetics. *Genetics*. 182:1089–1100. http://dx.doi.org/10.1534/genetics.109.103630

Oda, H., and S. Tsukita. 2001. Real-time imaging of cell-cell adherens junctions reveals that *Drosophila* mesoderm invagination begins with two phases of apical constriction of cells. *J. Cell Sci.* 114:493–501.

Rauzi, M., P.-F. Lenne, and T. Lecuit. 2010. Planar polarized actomyosin contractile flows control epithelial junction remodelling. *Nature*. 468:1110–1114. http://dx.doi.org/10.1038/nature09566

Royou, A., W. Sullivan, and R. Karess. 2002. Cortical recruitment of nonmuscle myosin II in early syncytial *Drosophila* embryos: its role in nuclear axial expansion and its regulation by Cdc2 activity. *J. Cell Biol.* 158:127–137. http://dx.doi.org/10.1083/jcb.200203148

Sammak, P.J., L.E. Hinman, P.O. Tran, M.D. Sjaastad, and T.E. Machen. 1997. How do injured cells communicate with the surviving cell monolayer? *J. Cell Sci.* 110:465–475.

Schirenbeck, A., T. Bretschneider, R. Arasada, M. Schleicher, and J. Faix. 2005. The Diaphanous-related formin dDia2 is required for the formation and maintenance of filopodia. *Nat. Cell Biol.* 7:619–625. http://dx.doi.org/10.1038/ncb1266

Shabir, S., and J. Southgate. 2008. Calcium signalling in wound-responsive normal human urothelial cell monolayers. *Cell Calcium*. 44:453–464. http://dx.doi.org/10.1016/j.ceca.2008.02.008

Simões, S. de M., J.T. Blankenship, O. Weitz, D.L. Farrell, M. Tamada, R. Fernandez-Gonzalez, and J.A. Zallen. 2010. Rho-kinase directs Bazooka/Par-3 planar polarity during *Drosophila* axis elongation. *Dev. Cell*. 19:377–388. http://dx.doi.org/10.1016/j.devcel.2010.08.011

Stramer, B., W. Wood, M.J. Galko, M.J. Redd, A. Jacinto, S.M. Parkhurst, and P. Martin. 2005. Live imaging of wound inflammation in *Drosophila* embryos reveals key roles for small GTPases during in vivo cell migration. *J. Cell Biol.* 168:567–573. http://dx.doi.org/10.1083/jcb.200405120

Sun, H.Q., M. Yamamoto, M. Mejillano, and H.L. Yin. 1999. Gelsolin, a multifunctional actin regulatory protein. *J. Biol. Chem.* 274:33179–33182. http://dx.doi.org/10.1074/jbc.274.47.33179

Tamada, M., T.D. Perez, W.J. Nelson, and M.P. Sheetz. 2007. Two distinct modes of myosin assembly and dynamics during epithelial wound closure. *J. Cell Biol.* 176:27–33. http://dx.doi.org/10.1083/jcb.200609116

Tian, L., S.A. Hires, T. Mao, D. Huber, M.E. Chiappe, S.H. Chalasani, L. Petreanu, J. Akerboom, S.A. McKinney, E.R. Schreiter, et al. 2009. Imaging neural activity in worms, flies and mice with improved GCaMP calcium indicators. *Nat. Methods*. 6:875–881. http://dx.doi.org/10.1038/nmeth.1398

Ueda, K., M. Murata-Hori, M. Tatsuka, and H. Hosoya. 2002. Rho-kinase contributes to diphosphorylation of myosin II regulatory light chain in nonmuscle cells. *Oncogene*. 21:5852–5860. http://dx.doi.org/10.1038/sj.onc.1205747

Wood, W., A. Jacinto, R. Grose, S. Woolner, J. Gale, C. Wilson, and P. Martin. 2002. Wound healing recapitulates morphogenesis in *Drosophila* embryos. *Nat. Cell Biol.* 4:907–912. http://dx.doi.org/10.1038/ncb875

Xu, S., and A.D. Chisholm. 2011. A Gαq-Ca^{2+} signaling pathway promotes actin-mediated epidermal wound closure in *C. elegans*. *Curr. Biol.* 21:1960–1967. http://dx.doi.org/10.1016/j.cub.2011.10.050

Yoo, S.K., C.M. Freisinger, D.C. LeBert, and A. Huttenlocher. 2012. Early redox, Src family kinase, and calcium signaling integrate wound responses and tissue regeneration in zebrafish. *J. Cell Biol.* 199:225–234. http://dx.doi.org/10.1083/jcb.201203154